Linda Ouma*, Agnes Pholosi and Martin Onani

Optimizing Cr(VI) adsorption parameters on magnetite (Fe_3O_4) and manganese doped magnetite ($Mn_xFe_{(3-x)}O_4$) nanoparticles

Abstract: Magnetite as an adsorbent is efficient since iron oxides have high affinities for heavy metal pollutants and are environmentally friendly. Manganese oxides provide catalytic properties which are desirable during the remediation of multi valent pollutants. Magnetite (Fe_3O_4) and manganese doped magnetite ($Mn_xFe_{(3-x)}O_4$) nanoparticles were synthesized and characterized to determine the manganese doping effects on magnetite's crystal and surface properties. Fe_3O_4 and $Mn_xFe_{(3-x)}O_4$ showed similarities in crystal morphology indicating that manganese doping did not alter the nature of Fe_3O_4 nanoparticles. Manganese doping improved magnetite's thermal properties as well as its surface area providing improved adsorption characteristics. The as-synthesized particles were applied in the optimization of hexavalent chromium adsorption. Adsorption proceeded under similar conditions for both adsorbents indicating their structural similarities. Higher efficiencies were observed on the doped adsorbent due to increased surface area and the presence of additional functional groups. Solution pH significantly affected the adsorption process aiding in the reduction of Cr(VI) ions to the less toxic Cr(III) species. The adsorption distribution coefficient K_D indicated that manganese doping significantly improved magnetite's affinity for hexavalent chromium. Adsorption and reduction were determined to responsible for pollutant reduction in solution at optimal conditions of pH 2, 5 g/L and 100 mg/L for adsorbent mass and solution concentration.

Keywords: adsorption; Fe_3O_4 nanoparticles; hexavalent chromium; manganese doping; multi-valent pollutants.

1 Introduction

Hexavalent chromium contamination of water is concerning due to its toxicity and mobility. Adsorption is a reliable, efficient and cost effective method for pollutant

***Corresponding author: Linda Ouma**, Department of Chemistry, University of the Western Cape, Private Bag X17, Bellville 7535, South Africa; and Department of Science, Technology and Engineering, Kibabii University, P. O. Box 1699, Bungoma 50200, Kenya, E-mail: oumachieng@gmail.com. https://orcid.org/0000-0002-4975-2495

Agnes Pholosi, Department of Chemistry, Vaal University of Technology, Private Bag X021, Vanderbijlpark 1900, South Africa

Martin Onani, Department of Chemistry, University of the Western Cape, Private Bag X17, Bellville 7535, South Africa

https://doi.org/10.1515/psr-2021-0149

sequestration and recovery [1]. The adsorption process however requires optimization to suit the individual adsorbent-adsorbate system as it is influenced by several variables [2]. A suitable adsorbent is a key consideration in designing suitable and efficient adsorption systems [3]. The adsorbent's properties include its pore size or porosity, particle size which has a bearing on crystallinity, colloidal stability, surface area and functionalization [4].

Magnetite nanoparticles are unique adsorbent materials owing to their magnetization ability which provides for easy retrieval [5]. They are composed of naturally occurring oxides which are ecofriendly and stable in nature. Additionally their surfaces are easily modified to provide for required surface groups [6, 7]. Controlling the size, homogeneity, crystallinity, and surface characteristics of these nanomaterials is possible owing to the preparation method used. For the synthesis of magnetite nanoparticles, there are numerous synthetic approaches. One of the most widely used methods is co-precipitation, which has advantages over other techniques, such as minimal cost, low energy requirements, high product integrity, and particle homogeneity [6]. Magnetite synthesis through ferrous (Fe^{2+}) and ferric (Fe^{3+}) co-precipitation in the presence of excess hydroxyl ions proceeds according to equation (1) [7].

$$Fe^{2+} + 2Fe^{3+} + 8OH^- \rightarrow Fe_3O_4 + 4H_2O \quad (1)$$

Magnetite doping is considered a promising option to improve its affinity towards pollutants since doping has been reported to improve metal oxides' properties [8]. Manganese doping increases magnetite's affinity for pollutants as well as improving its magnetic properties. Divalent manganese cations consist of five unpaired electrons which are responsible for its paramagnetism [9]. This property increases the magnetic susceptibility of magnetite which is a superparamagnetic material [10]. As a result, a material composed of iron and manganese oxides would be superior in terms of both pollutant affinities and magnetic retrieval properties. However, to attain the required properties and composition, doping needs to be monitored carefully [3, 9]. The effects of manganese doping on magnetite adsorption were studied and reported in a previous study, the results from that study informed the dopant concentration applied herein [3].

To optimize the adsorption of hexavalent chromium (Cr(VI)) on Magnetite (Fe_3O_4) and Manganese doped magnetite ($Mn_xFe_{(3-x)}O_4$), their affinities were evaluated under varying conditions. The evaluation provided for the determination of optimal conditions for adsorbate concentration reduction while efficiently utilizing the adsorbent hence maximizing adsorption capacity. This chapter reports on the synthesis, characterization and optimization of hexavalent chromium adsorption onto the aforementioned adsorbents.

2 Experimental

2.1 Materials

Reactants used in this study were ammonium hydroxide (25%), potassium dichromate (>99%) and sodium hydroxide (>98%) from ACE Chemicals, South Africa. Hydrochloric acid (32%), ferrous sulphate (>98%) and ferric chloride (>99%) from Merck, Germany. All chemicals were used without any further purification.

2.2 Methods

2.2.1 Magnetite synthesis: Magnetite nanoparticles were prepared following a one-pot co-precipitation procedure as described in an earlier study [10]. Deionised water was heated under vacuum with continuous stirring at 80 °C for 15 min and nitrogen gas for a further 15 min to maintain an inert atmosphere. Iron salts ($FeCl_3.6H_2O$ and $FeSO_4.7H_2O$) were separately dissolved in deionized water and introduced into the solution, ammonium hydroxide was added as a precipitating agent with continuous stirring till a black precipitate was formed. The precipitated particles were washed with deionized water, rinsed with ethanol and dried under vacuum to prevent further oxidation. Doping was achieved by adding manganese sulphate solution then precipitated *in situ* with ferric and ferrous ions to achieve the desired dopant concentration of $Mn_{0.06}Fe_{2.94}O_4$ [3]. The optimization of manganese dopant concentration was described in detail in a previous study [3].

2.2.2 Characterization: Various analytical techniques were used to characterize the samples in order to determine their composition, crystal properties and dopant effects. X-ray diffraction (XRD) analysis was used to determine the particles' crystal properties and dopant effects on the crystal structure. An advanced diffractometer (Bruker AXS D8; Cu Kα (λ = 1.5418 Å)) was used for the analysis. A PerkinElmer Fourier transform infrared spectrometer (400 FT-IR/NIR) was used to characterize the adsorbent surface and dopant effects on the magnetite surface functionalization while a thermogravimetric analyser (PerkinElmer TGA 4000) was used in thermal degradation investigation. Perkin Elmer (Lambda 25) UV–Vis spectrophotometer and Shimadzu AA 7000 (air/acetylene flame, λ = 357.9 nm) were used for UV–Vis spectroscopy and atomic absorption analysis, respectively.

2.2.3 Adsorption: Potassium dichromate was dissolved in deionized water to prepare a Cr(VI) stock solution. Hydrochloric acid and sodium hydroxide (0.1 M) were used to achieve desired solution pH. Hexavalent chromium concentration was determined by complexation with 1,5-diphenylcarbazide resulting in a pink complex which was analysed on a UV–Vis at 540 nm [11]. Atomic absorption spectrophotometry was applied in total chromium concentration determination while trivalent chromium concentration was indirectly determined as the difference between the total and hexavalent chromium concentrations. Adsorbent dose effects were studied by using adsorbent masses ranging between 0.1 and 1 g. The effect of solution concentration was studied between 25 and 150 mg/L.

3 Results and discussions

3.1 Characterization

Figure 1 depicts the XRD pattern of as-synthesised Fe_3O_4 and $Mn_{0.06}Fe_{2.94}O_4$ nanoparticles. The pattern reveals crystalline plane peaks with the indicated miller indices for each peak: 30.75° (220), 36.09° (311), 43.81° (400), 54.03° (422), 57.67° (511) and 63.26° (440). The pattern compares well with the Joint committee for powder diffraction (JCPDS) file No. 19-0629 (Figure 1) confirming the as-synthesized magnetite nanoparticles' inverse spinel structure [12].

Manganese doping was performed to improve the adsorbent's redox properties and was deemed a suitable dopant due to its charge and size. The doped nanoparticles retained the characteristic magnetite peaks without the formation of any secondary phases implying that manganese was incorporated into the magnetite lattice [3]. Manganese resulted in slight shifts to lower diffraction angles as observed from the major plane (311). The shift indicates that manganese slightly altered the crystalline plane resulting in slight increases in the crystals' lattice parameter and cell volume [3, 13].

The infrared spectrum of magnetite nanoparticles is depicted in Figure 2, revealing the appearance of hydroxyl surface functional groups attributed to adsorbed water. The surface hydroxyl groups allow amphoteric reactions on the oxide surfaces depending on the solution pH [4]. As indicated the oxide surfaces are protonated and

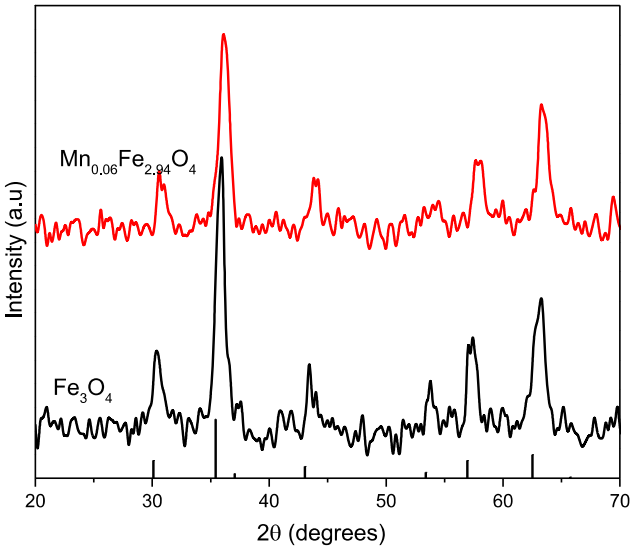

Figure 1: Powder X-ray diffraction patterns of magnetite and manganese doped magnetite with reference peaks (JCPDS Card 19-0629).

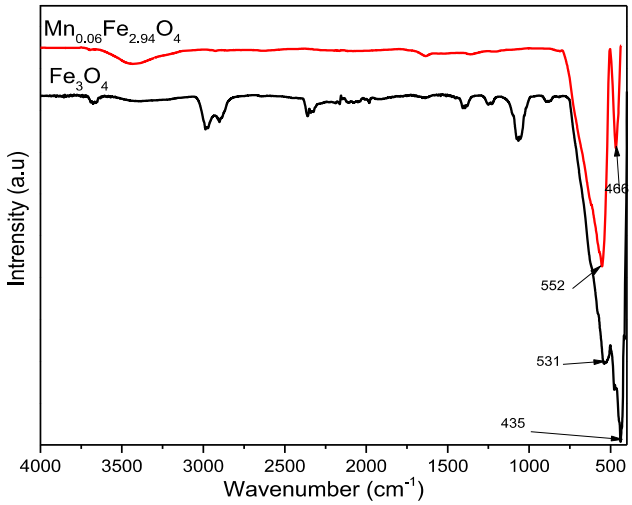

Figure 2: FT-IR spectra of synthesized samples (Fe_3O_4 and $Mn_{0.06}Fe_{2.94}O_4$).

deprotonated as solution pH is raised. The Fe-O surface group assigned to 435 cm^{-1} confirmed iron oxidation forming iron oxide particles [6]. Manganese substitution in the iron oxide structure caused the Fe-O peak to shift to 466 cm^{-1} from 435 cm^{-1}, while the appearance of Mn-substitution at 552 cm^{-1} on the iron oxide surface affirmed manganese doping. Manganese substitution affirms diffraction results indicating manganese substitution in the Fe_3O_4 lattice [14, 15].

Thermal analysis curves for the as-synthesized materials are shown in Figure 3. From the data, the samples underwent thermal decomposition in stages, initially

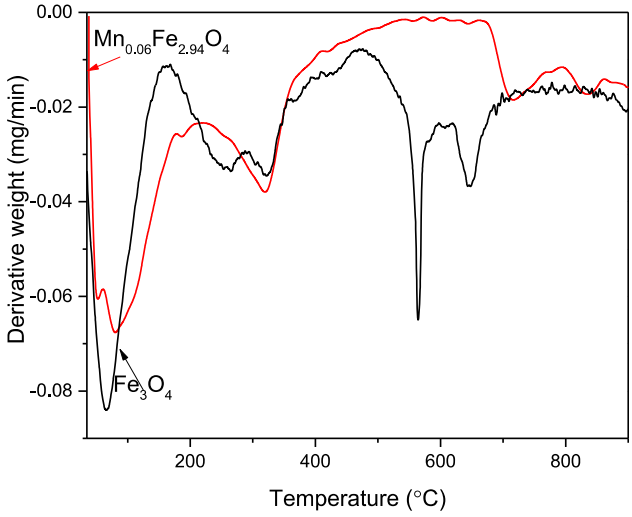

Figure 3: DTA curves for Fe_3O_4 and $Mn_{0.06}Fe_{2.94}O_4$ nanoparticles.

losing surface bound water followed by the loss of pore bound water and dihydroxylation [16]. Finally the Fe_3O_4 sample was reduced to FeO and Fe after deoxidation [6]. At higher temperatures, the decomposition profile of doped magnetite nanoparticles ($Mn_{0.06}Fe_{2.94}O_4$) revealed slight differences from Fe_3O_4. Manganese substitution in the Fe_3O_4 lattice resulted in higher temperatures for magnetite reduction and deoxidation (approx. 700 °C). It also presented an additional decomposition stage at approximately 830 °C attributed to manganese oxide deoxidation [15].

The isoelectric points for the Fe_3O_4 and $Mn_{0.06}Fe_{2.94}O_4$ nanoparticles used in this study were reported previously as pH 7.1 and pH 6.8 respectively while the BET surface areas were 113 and 127 m^2/g, respectively [3]. In the same study, the pore sizes of Fe_3O_4 were observed to decrease upon manganese substitution due to the partial replacement of the smaller Fe ions with the larger Mn ions [17]. The incorporation of manganese into the magnetite lattice resulted in increased adsorption sites as evident from the increased surface area. Manganese oxide has been applied in the adsorption of chromium from water and its incorporation in activated alumina was reported to improve the adsorption properties of both adsorbents [18]. The presence of Mn-O sites in the $Mn_{0.06}Fe_{2.94}O_4$ adsorbent would therefore provide additional adsorption sites therefore improving its efficiency.

3.2 Adsorption optimization

Adsorption process is dependent on binding on the adsorbent surface and its properties, however chromium adsorption is also influenced by surface redox reactions since it exists in multiple stable oxidation states [19]. Redox reactions at the adsorbent surface are greatly influenced by surface properties as well as solution properties including pH and concentration. One factor at a time (OFAT) experimental design was applied to determine the effects of adsorbent quantities, solution pH and concentration on the efficiency of hexavalent chromium (Cr(VI)) adsorption onto magnetite and manganese doped magnetite nanoparticles. The effect of redox reactions was also determined by determining trivalent chromium (Cr(III)) concentrations in solution. The % efficiency of adsorption and adsorbent capacity were calculated following equations (2) and (3) [20].

$$E = \left[\frac{(C_0 - C_t)}{C_0}\right] \times 100\% \tag{2}$$

$$q = (C_0 - C_t)\ x\ \frac{V}{m} \tag{3}$$

where E is the adsorption efficiency (%), q is the adsorption capacity, C_0 and C_t are the solution concentrations pre and post adsorption, V is the solution volume and m is the adsorbent dose.

Chromium speciation in solution is pH dependent thus influences adsorption properties at varied pH ranges [20]. Solution pH also has a significant influence on the adsorption process since it affects electrostatic attraction and surface binding [3]. Both iron and manganese oxides have amphoteric surface groups that protonate and deprotonate as solution pH is raised. At acidic pH ranges electrostatic attraction is majorly responsible for binding anionic $HCrO_4^-$ to protonated surface groups [14, 21]. Figure 4a shows Cr(VI) adsorption efficiency as a factor of solution pH. As pH increases, the binding capacity of the adsorbents decrease as a result of the increasing negative charge on the adsorbent surface causing repulsion with anionic chromium species.

Figure 4b shows the concentration of trivalent chromium species when adsorption is performed at varying pHs. The highest reduction in Cr(VI) concentration was observed at pH 1 while simultaneously observing the highest concentration of Cr(III) in solution. The reduction in Cr(VI) concentration was therefore largely attributed to surface reduction hence pH 2 was selected as the optimal pH. Ferrous ions in magnetite assist in surface reduction of hexavalent chromium, the resulting trivalent ions are then either released into the solution (Figure 4b) or bound on the surface through complexation [21, 22]. As the solution becomes more basic, lower concentrations of trivalent ions are recorded (Figure 4b). This results from increased binding sites and electrostatic attraction between the increasingly anionic surface and the cationic trivalent species in solution [23].

The binding of Cr(III) ions was more efficient on $Mn_{0.06}Fe_{2.94}O_4$ surfaces as compared to Fe_3O_4 surfaces with the highest Cr(III) sequestration occurring at pH 6 (Fe_3O_4) and pH 8 ($Mn_{0.06}Fe_{2.94}O_4$) where the surface complexation was highest [24]. Improved binding of Cr(III) on the doped adsorbent surface was due to the presence of lone pairs of electrons on MnO_2 species [4, 24]. Malek et al. and Xiong et al. observed improved adsorbent properties resulting from manganese incorporation similar to the observations in the current study [15, 25].

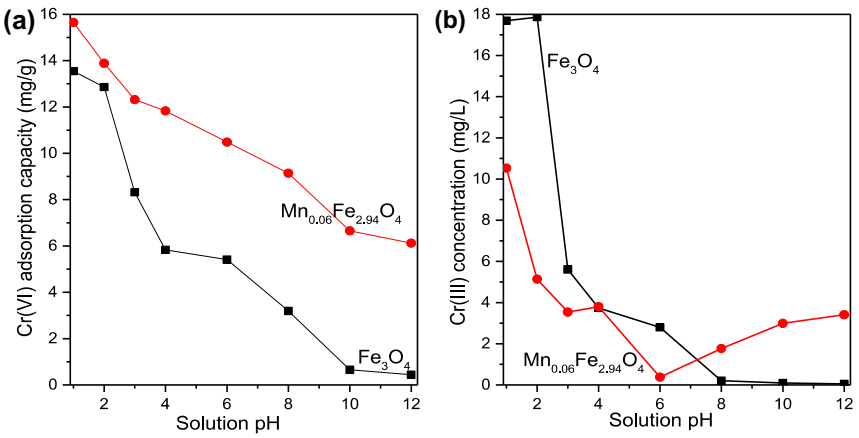

Figure 4: Effect of solution pH on (a) Cr(VI) adsorption capacity on $Mn_{0.06}Fe_{2.94}O_4$ and Fe_3O_4 and (b) Cr(III) formation in solution.

The quantity of adsorbent that comes into contact with the adsorbate impacts uptake and is thus significant in determining the best possible adsorption conditions. As the adsorbent dosage increases, so do the adsorption sites, increasing adsorption efficiency [19]. However, at low adsorbent doses, high sorption capacity is observed due to adsorbate molecules competing for limited binding sites (Figure 5). With a fixed adsorbate concentration, increasing the adsorbent dose provides more adsorption sites resulting in decreased saturation. This in turn leads to lower adsorbent capacities [2, 19]. To maintain optimal efficiencies with desirable capacities, 5 g/L was selected from the tested values to be used for further experiments since it provided moderate efficiencies while not adversely affecting the adsorption capacities.

The adsorbent efficiency can further be described by a solid-phase distribution coefficient K_D. K_D calculates the partition coefficient of the adsorbate between the solid (adsorbent surface) and solution phases according to equation (4) [26].

$$K_D = \frac{C_0 - C_e}{C_e} x \frac{V}{m} \tag{4}$$

where K_D, C_0 and C_e refer to the distribution coefficient, initial and equilibrium Cr(VI) concentrations, V and m refer to the solution volume in milliliters adsorbent mass in grams. Its value indicates the adsorbent's affinity to the target species under the specified conditions, higher values therefore point to a more efficient adsorbent material. Figure 5 shows the adsorption efficiencies of the adsorbents with increasing adsorbent mass. It indicates that manganese significantly increases magnetite's affinity towards Cr(VI) ions. The slight decrease in K_D values at lower doses was attributed to increased competition for active sites resulting in decreased complexation ability as some of the sites were involved in chromium reduction [26].

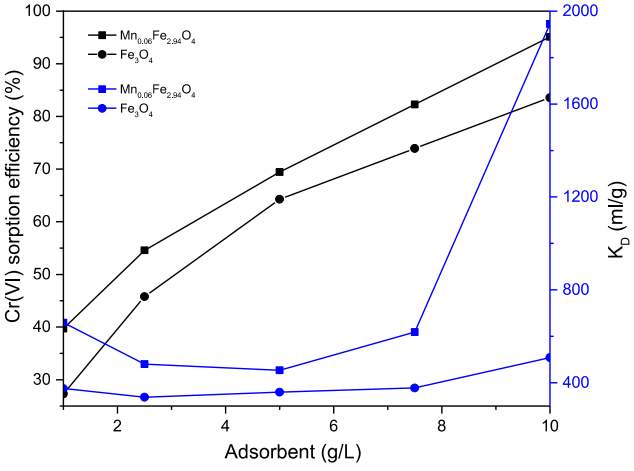

Figure 5: Cr(VI) sorption efficiency on Fe_3O_4 and $Mn_{0.06}Fe_{2.94}O_4$ and adsorption distribution coefficient with increasing adsorbent doses.

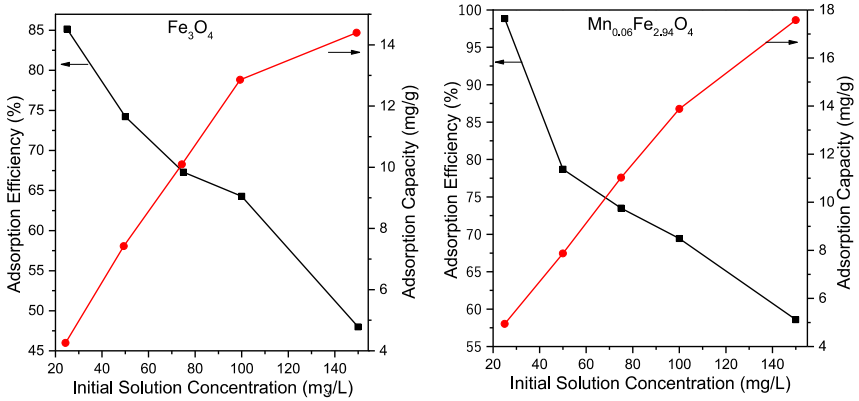

Figure 6: Effect of solution concentration on Cr(VI) adsorption.

Adsorbate concentration is a critical factor in determining optimal adsorption parameters since the solution concentration influences the efficiency of the adsorption process. Figure 6 shows that higher solution concentrations resulted in increased adsorption per unit mass of adsorbent. The observation was attributed to greater adsorbate mass transfer from solution to the solid phase as adsorbate ions were increased while surfaces remained constant. Increased mass transfer improved the interaction and complexation between adsorbate ions and adsorbent surfaces [10].

Increasing the solution concentration resulted in lower % efficiencies owing to the increased chromium molecules in solution [27, 28]. The decrease was caused by adsorbent saturation therefore, further increasing the chromium concentration would not result in a significant increase in surface complexation [12]. 100 mg/L was considered as the optimal solution concentration since both adsorption efficiency and capacity were optimized.

4 Conclusions

Magnetite (Fe_3O_4) and manganese doped magnetite ($Mn_{0.06}Fe_{2.94}O_4$) nanoparticles were synthesized via a one-pot co-precipitation technique and applied in the determination of optimum parameters for Cr(VI) adsorption. The particles diffraction data was consistent with the inverse cubic spinel structure of synthetic magnetite. Manganese was incorporated into iron lattice through the formation of a solid solution with magnetite resulting in a uniform phase with no secondary phases being observed. Cr(VI) adsorption on both adsorbents was optimized and all the tested factors had consistent results for Fe_3O_4 and $Mn_{0.06}Fe_{2.94}O_4$ with the latter providing higher affinities, efficiencies and capacities. The improved performance was due to increased adsorption sites provided by manganese oxides on the adsorbent surface and lone

pairs of electrons responsible for chromium reduction and binding on the surface. Magnetite modification provided a cost effective adsorbent for pollutant remediation through surface sequestration and redox reactions producing the less toxic Cr(III) species.

Acknowledgements: The authors acknowledge financial support from South Africa's National Research Foundation (NRF).
Author contributions: All the authors have accepted responsibility for the entire content of this submitted manuscript and approved submission.
Research funding: National Research Foundation.
Conflict of interest statement: The authors declare no conflicts of interest regarding this article.

References

1. Luo J, Meng X, Crittenden J, Qu J, Hu C, Liu H, et al. Arsenic adsorption on α-MnO_2 nanofibers and the significance of (1 0 0) facet as compared with (1 1 0). Chem Eng J 2018;331:492–500.
2. Santra D, Sarkar M. Optimization of process variables and mechanism of arsenic (V) adsorption onto cellulose nanocomposite. J Mol Liq 2016;224:290–302.
3. Ouma L, Ofomaja A. Probing the interaction effects of metal ions in $Mn_xFe_{(3-x)}O_4$ on arsenite oxidation and adsorption. RSC Adv 2020;10:2812–22.
4. Ouma L, Onani M. Sequestration of heavy metal pollutants by Fe_3O_4-based composites. In: Lichtfouse E, Muthu SS, Khadir A, editors. Inorganic-organic compos. water wastewater treat. Singapore: Springer Singapore; 2022:101–16 pp.
5. Pholosi A, Naidoo EB, Ofomaja AE. Batch and continuous flow studies of Cr(VI) adsorption from synthetic and real wastewater by magnetic pine cone composite. Chem Eng Res Des 2020;153: 806–18.
6. Masuku M, Ouma L, Pholosi A. Microwave assisted synthesis of oleic acid modified magnetite nanoparticles for benzene adsorption. Environ Nanotechnol Monit Manag 2021;15:100429.
7. Roth H-C, Schwaminger SP, Schindler M, Wagner FE, Berensmeier S. Influencing factors in the co-precipitation process of superparamagnetic iron oxide nano particles: a model based study. J Magn Magn Mater 2015;377:81–9.
8. Yuan Z, Liu B, Zhou P, Zhang Z, Chi Q. Aerobic oxidation of biomass-derived 5-hydroxymethylfurfural to 2,5-diformylfuran with cesium-doped manganese dioxide. Catal Sci Technol 2018;8:4430–9.
9. Yang L, Ma L, Xin J, Li A, Sun C, Wei R, et al. Composition tunable manganese ferrite nanoparticles for optimized T_2 contrast ability. Chem Mater 2017;29:3038–47.
10. Ouma ILA, Naidoo EB, Ofomaja AE. Iron oxide nanoparticles stabilized by lignocellulosic waste as green adsorbent for Cr(VI) removal from wastewater. Eur Phys J Appl Phys 2017;79:30401.
11. Bishop ME, Glasser P, Dong H, Arey B, Kovarik L. Reduction and immobilization of hexavalent chromium by microbially reduced Fe-bearing clay minerals. Geochem Cosmochim Acta 2014;133: 186–203.
12. Rajput S, Pittman CU, Mohan D. Magnetic magnetite (Fe_3O_4) nanoparticle synthesis and applications for lead (Pb^{2+}) and chromium (Cr^{6+}) removal from water. J Colloid Interface Sci 2016; 468:334–46.

13. Akl AAS, Elhadi M. Estimation of crystallite size, lattice parameter, internal strain and crystal impurification of nanocrystalline $Al_3Ni_{20}B_x$ alloy by williamson-hall method. J Ovonic Res 2020;16: 323–35.
14. Liu Y, Luo C, Cui G, Yan S. Synthesis of manganese dioxide/iron oxide/graphene oxide magnetic nanocomposites for hexavalent chromium removal. RSC Adv 2015;5:54156–64.
15. Malek TJ, Chaki SH, Chaudhary MD, Tailor JP, Deshpande MP. Effect of Mn doping on Fe_3O_4 nanoparticles synthesized by wet chemical reduction technique. Iran J Energy Environ 2018;9: 121–9.
16. Otieno BO, Apollo SO, Naidoo BE, Ochieng A. Photodecolorisation of melanoidins in vinasse with illuminated TiO_2-ZnO/activated carbon composite. J Environ Sci Heal 2017;52:616–23.
17. Güner S, Amir M, Geleri M, Sertkol M, Baykal A. Magneto-optical properties of Mn3+ substituted Fe3O4 nanoparticles. Ceram Int 2015;41:10915–22.
18. Punia S, Wu L, Khodadoust AP. Adsorption of hexavalent chromium from water using manganese-aluminum coated sand: kinetics, equilibrium, effect of pH and ionic strength. J Environ Sci Heal Part A 2021;56:334–45.
19. Roy P, Dey U, Chattoraj S, Mukhopadhyay D. Modeling of the adsorptive removal of arsenic (III) using plant biomass: a bioremedial approach. Appl Water Sci 2017;7:1307–21.
20. Padmavathy KS, Madhu G, Haseena PV. A study on effects of pH, adsorbent dosage, time, initial concentration and adsorption isotherm study for the removal of hexavalent chromium (Cr (VI)) from wastewater by magnetite nanoparticles. Procedia Technol 2016;24:585–94.
21. Fathy NA, El-Wakeel ST, Abd El-Latif RR. Biosorption and desorption studies on chromium (VI) by novel biosorbents of raw rutin and rutin resin. J Environ Chem Eng 2015;3:1137–45.
22. Ouma ILA, Naidoo EB, Ofomaja AE. An insight into the adsorption mechanism of hexavalent chromium onto magnetic pine cone powder. Chem. a Clean Heal. Planet. Cham: Springer International Publishing; 2019:185–95 pp.
23. Pan J, Jiang J, Xu R. Adsorption of Cr(III) from acidic solutions by crop straw derived biochars. J Environ Sci 2013;25:1957–65.
24. Wassie AB, Srivastava VC. Teff straw characterization and utilization for chromium removal from wastewater: kinetics, isotherm and thermodynamic modelling. J Environ Chem Eng 2016;4: 1117–25.
25. Xiong T, Yuan X, Cao X, Wang H, Jiang L, Wu Z, et al. Mechanistic insights into heavy metals affinity in magnetic MnO_2@Fe_3O_4/poly(m-phenylenediamine) core–shell adsorbent. Ecotoxicol Environ Saf 2020;192:110326.
26. Zolfaghari G. β-Cyclodextrin incorporated nanoporous carbon: host–guest inclusion for removal of p-Nitrophenol and pesticides from aqueous solutions. Chem Eng J 2016;283:1424–34.
27. Ouma ILA, Mushonga P, Onani MO. Effects of reaction parameters on the growth and optical properties of PbSe nanocrystals. J Nano Res 2015;34:79–89.
28. Zhang J, Lin S, Han M, Su Q, Xia L, Hui Z. Adsorption properties of magnetic magnetite nanoparticle for coexistent Cr(VI) and Cu(II) in mixed solution. Water 2020;12:446.